HEALTH AND MEDICINE

Accessing neuroinflammation sites: Monocyte/neutrophil-mediated drug delivery for cerebral ischemia

Jia Hou[1,2,3,4]*, Xu Yang[5]*, Shiyi Li[1], Zhekang Cheng[1,2], Yuhua Wang[6], Jing Zhao[7], Chun Zhang[1], Yongji Li[3], Man Luo[3], Hongwei Ren[1], Jianming Liang[1], Jue Wang[1], Jianxin Wang[1,2†], Jing Qin[1,2†]

Cerebral ischemia (CI) results from inadequate blood flow to the brain. The difficulty of delivering therapeutic molecules to lesions resulting from CI hinders the effective treatment of this disease. The inflammatory response following CI offers a unique opportunity for drug delivery to the ischemic brain and targeted cells because of the recruitment of leukocytes to the stroke core and penumbra. In the present study, neutrophils and monocytes were explored as cell carriers after selectively carrying cRGD liposomes, which effectively transmigrated the blood-brain barrier, infiltrated the cerebral parenchyma, and delivered therapeutic molecules to the injured sites and target cells. Our results showed the successful comigration of liposomes with neutrophils/monocytes and that both monocytes and neutrophils were important for successful delivery. Enhanced protection against ischemic injury was achieved in the CI/reperfusion model. The strategy presented here shows potential in the treatment of CI and other diseases related to inflammation.

INTRODUCTION

Cerebral ischemia (CI) is a pathological condition involving a severe reduction of blood flow to the brain caused by heart arrest or occluded blood vessels, leading to a failure to cellularly meet metabolic demands. The shortage of blood flow leads to insufficient oxygen supply to the brain tissue and causes an ischemic stroke (*1*, *2*). The standard treatment for acute CI is the administration of thrombolytic drugs that break down the blood clots to restore blood supply to the affected areas. However, the therapeutic window of such treatment is limited and within only 3 to 4.5 hours of symptom onset. Furthermore, less than 3% of all patients that suffer from ischemic strokes in the United States receive thrombolytic therapy for various reasons (*3*, *4*). Once the therapeutic "time window" is missed, thrombolytic treatment is no longer recommended because of potential safety issues. The resulting pathological condition of the brain vessels poses a great challenge to the treatment of patients after acute CI, when the use of neuroprotective agents such as edaravone (ER) could potentially protect neuronal cells by scavenging free radicals (*5*, *6*). However, drug concentrations could be suboptimal in ischemic areas owing to insufficient blood supply to affected regions, thereby severely compromising the therapeutic efficacy of the neuroprotective agents (*7*). Although some breakdown of the blood-brain barrier (BBB) is found in both ischemic and nonischemic areas (*8*, *9*), it is still insufficient for selective accumulation of drugs in the impaired parenchyma. Hence, after decades of research, neuroprotective agents that showed promise in preclinical experiments have failed to translate to clinical benefits (*10*, *11*).

Studies on both human and animal have shown secondary inflammation following an ischemic insult. The inflammatory response after CI involves the recruitment of leukocytes [mainly monocytes and neutrophils (M/Ns)] to the stroke core and penumbra (*12*, *13*). This delayed process occurs in the infarcted hemisphere from 30 min to a minimum of 1 week after the onset of a stroke in both humans and animals (*14*, *15*). Emerging studies have reported how nanotherapeutics capture immune cells as delivery vehicles to target damaged or inflammatory tissues (*16*, *17*). Therefore, secondary inflammation offers a unique therapeutic opportunity (*18*, *19*) by extending the window after CI and enabling the effective delivery of therapeutic molecules to ischemic subregions and targeted cells in the brain. Immune cell–based delivery exhibits a different kinetic profile in comparison to that of conventional carriers used in drug delivery. The use of immune cells as potential carrier cells could facilitate the delivery of drugs to ischemic areas despite low blood flow rates or occluded vessels.

In this study, we exploited leukocytes (M/Ns) as potential molecular "Trojan horses" for drug delivery to ischemic subregions and target cells to alleviate ischemic injuries. This could be hypothetically achieved by engineering liposomes that actively target cell surface receptors on M/Ns, which are thus triggered following internalization and ligand/receptor binding. We selected cRGD peptide [cRGD, cyclo (Arg-Gly-Asp-D-Tyr-Lys)] as the targeting ligand for the M/Ns, as the cRGD peptide is widely known to be recognized by integrin $\alpha_v\beta_1$ (*20*), which is highly expressed on the surface of M/Ns (*21*–*23*). Moreover, the binding of cRGD and integrin $\alpha_v\beta_1$ could efficiently trigger the internalization of receptors, ligands, and the carriers that are modified with the ligands. Liposomes coupled with cRGD (cRGDLs) can be preferentially presented to blood M/Ns and taken up into the penumbra in the ischemic brain, which would enhance the protection against ischemic stroke.

RESULTS AND DISCUSSION

Binding affinity assay with surface plasmon resonance

The binding affinity of the cRGD peptide for the targeted receptor αvβ1 was first confirmed using surface plasmon resonance (SPR). We

[1]Department of Pharmaceutics, School of Pharmacy, Fudan University, Key Laboratory of Smart Drug Delivery, Ministry of Education, Shanghai 201203, China. [2]Institutes of Integrative Medicine of Fudan University, Shanghai 200040, China. [3]Department of Pharmaceutics, School of Pharmacy, Heilongjiang University of Chinese Medicine, Harbin, Heilongjiang Province 150040, China. [4]Department of Pharmacy, Municipal Hospital, Ministry of Healthcare, Weihai, Shandong Province 264200, China. [5]Department of Pharmacy, THe Fifth People's Hospital of Shanghai, Fudan University, Shanghai 200240, China. [6]Division of Molecular Pharmaceutics, Eshelman School of Pharmacy, University of North Carolina at Chapel Hill, Chapel Hill, NC 27599, USA. [7]Minhang Hospital, Fudan University, Shanghai 201199, China.
*These authors contributed equally to this work.
†Corresponding author. Email: jxwang@fudan.edu.cn (J.W.); qinjing@fudan.edu.cn (J.Q.)

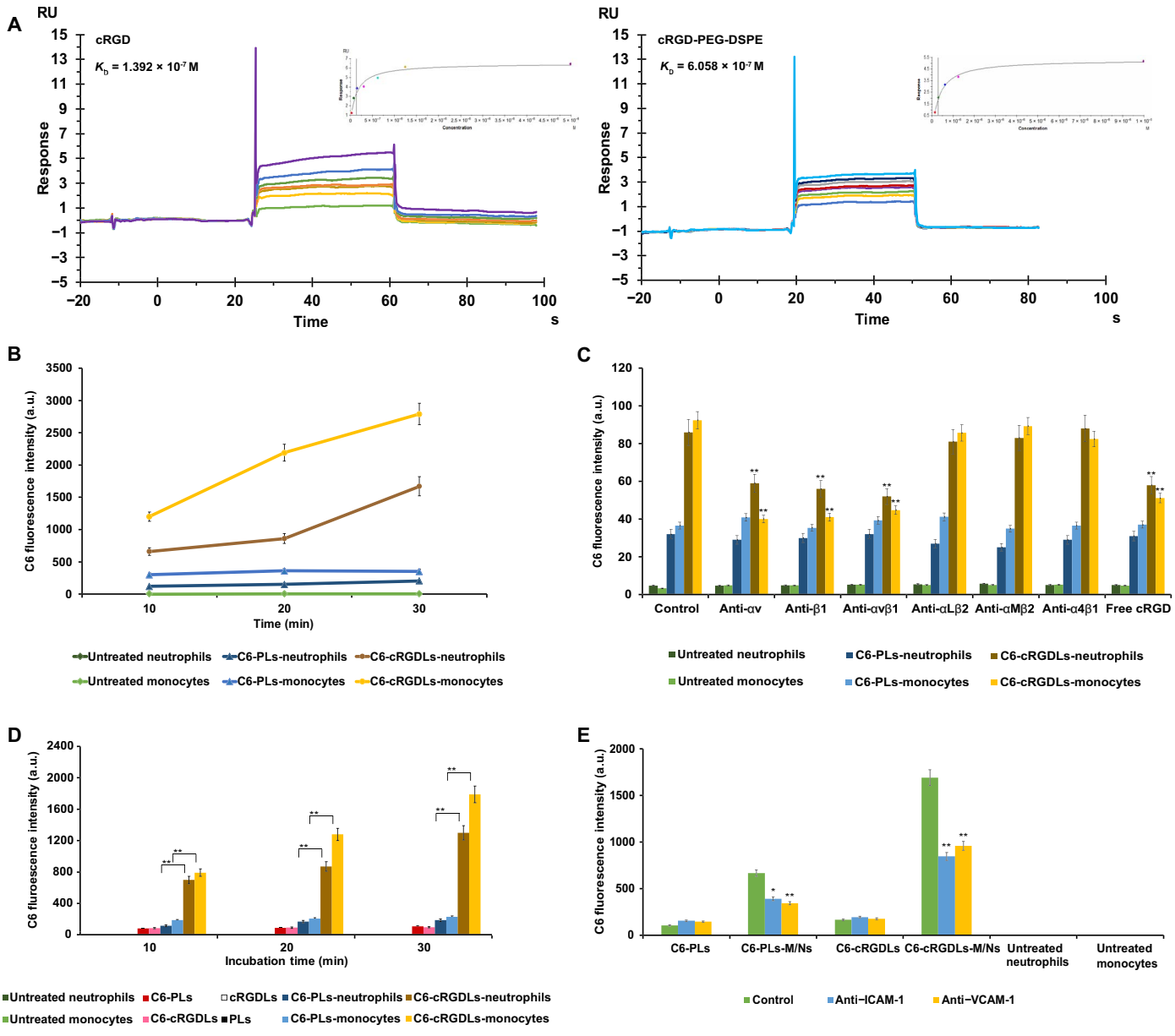

Fig. 1. The uptake characterization and comigration across HBMEC of liposomes with M/Ns. (**A**) Binding affinity assay of cRGD/cRGD-PEG-DSPE with αvβ1 protein using SPR. RU, Response Unit. (**B**) The uptake of C6-PLs/C6-cRGDLs by M/Ns after 30 min of incubation assayed by flow cytometer. a.u., arbitrary unit. (**C**) Effects of blocking antibodies against integrins and free cRGD peptide on uptake of C6-PLs/C6-cRGDLs with M/Ns assayed by flow cytometer. $^{**}P < 0.01$, compared with control. (**D**) The C6 fluorescence of the suspension in the lower chamber after the migration of C6-PLs/C6-cRGDLs across HBMEC with or without M/Ns assayed by microplate reader. PLs and cRGDLs meant non–fluorescence-labeled liposomes. $^{**}P < 0.01$. (**E**) The C6 fluorescence of the suspension in lower chamber with treatment of blocking antibodies against ICAM-1 or VCAM-1 on HBMEC assayed by microplate reader. $^{**}P < 0.01$ and $^{*}P < 0.05$, compared with control. All untreated neutrophils and monocytes in (A) to (D) meant blank cell controls untreated with liposomes.

determined that cRGD and cRGD–polyethylene glycol (PEG)–distearoyl phosphoethanolamine (DSPE) exhibited fast binding and dissociation with the αvβ1 protein (Fig. 1A). The interaction between cRGD/cRGD-PEG-DSPE and the αvβ1 protein was dose dependent, and the equilibrium dissociation constant (K_D) values were 1.392×10^{-7} and 6.058×10^{-7}, respectively, indicating that cRGD has a strong affinity for αvβ1 protein. Although PEG-DSPE exerted a little influence on the affinity of the cRGD peptide, the K_D value was still at a high level. Hence, cRGD peptide (5% molar ratio of lipid) was a target ligand in the present study.

Characterization of liposomes

All the liposomes described in the present study were composed of the same lipid components: soy phospholipid (SPC), DSPE-PEG (PEG-3400), distearoyl phosphatidyl glycerol (DSPG), and cholesterol (Chol) (SPC:DSPG:Chol:DSPE-PEG 85:5:10:5 molar ratio). The liposomes were presented as either plain forms (PLs) or targeting forms (cRGDLs) by completely replacing DSPE-PEG with 5 mol% cRGD-PEG-DSPE. The successful synthesis of cRGD-PEG-DSPE was confirmed using matrix-assisted laser desorption/ionization–time-of-flight

(fig. S1). A passive drug-loading method was used to prepare ER-loaded PLs (ER-PLs) or cRGDLs (ER-cRGDLs). The loading of drug or fluorescent dye (0.5 mol%) did not affect the physicochemical properties and stability of the liposomes (fig. S2 and table S1). The encapsulation efficiency of ER was approximately 75% for both ER-PLs and ER-cRGDLs, with a mean particle size of 150 nm and zeta potential of −26 mV. Both blank and drug-loaded liposomes were stable for up to 1 week at 4°C under nitrogen regardless of surface modification.

To characterize the dispersion properties of the liposomes, we incubated PLs and cRGDLs with a cell culture medium (Dulbecco's modified Eagle's medium, supplemented with 10% fetal bovine serum or 10, 30, or 50% serum) for 30 min. We observed no significant differences in the particle sizes between the different types of media or different positions of the culture dishes and test tubes (figs. S3 and S4). Scattering intensity was closely related to the particle concentration and refraction coefficient and was evaluated by measuring the derived account rate, which changed when obvious accumulation or precipitation occurred (*24*). In the present study, the derived count rates were not significantly different between the samples from different positions in the same medium, whereas they changed considerably in the presence of different types of media. These results demonstrated that the observed change in scattering intensity was the result of the refraction coefficient of the medium and not from the uneven dispersion of PLs or cRGDLs in the medium. Hence, the PLs and cRGDLs were uniformly dispersed in all types of the tested media.

Characteristics of the uptake of cRGDLs by M/Ns in vitro

An in vitro cell uptake study was performed to validate the premise that the presence of cRGD on the surface of liposomes facilitates the uptake of cRGDLs by M/Ns. M/Ns were isolated from the anticoagulant-treated peripheral blood of rats. Coumarin 6 (C6) was loaded into PLs (C6-PLs) or cRGDLs (C6-cRGDLs) as a fluorescent marker. C6-PLs or C6-cRGDLs were incubated with M/Ns for 30 min at 37°C. As expected, the cRGD peptide significantly enhanced the uptake of liposomes by cells. Unlike C6-PLs, C6-cRGDLs showed up to an 8.1-fold increase in fluorescence intensity for neutrophils and up to a 7.9-fold increase for monocytes (Fig. 1B).

To assay the uptake efficiency of liposomes, sulfo-cyanine5 carboxylic acid (Cy5)–labeled cRGDLs and PLs were incubated with M/Ns for 30 min. Free liposomes were removed by washing with phosphate-buffered saline (PBS). As a result, we determined that the uptake efficiency of cRGDLs was 82.7%, while that of PLs was 12.1%. In addition, to confirm the localization of liposomes in M/Ns, cRGDLs or PLs were labeled with phosphoethanolamine-*N*-(7-nitro-2-1,3 benzoxadiazol-4-yl) (NBD-PE) on the bilayer of liposome membranes and loaded with hydrophilic Cy5 in the internal phase of liposomes for tracking purpose. Following the incubation of M/Ns with liposomes, M/Ns were visualized using confocal scanning laser microscopy (CSLM, fig. S10). The colocalization of both Cy5 and NBD-PE markers was observed in M/Ns. The fluorescence intensity of cRGDLs was much higher than that of PLs. The dual-labeling analysis of the cellular levels confirmed that most of the cRGDLs were taken up and retained as intact nanocarriers by M/Ns.

The enhanced uptake of C6-cRGDLs was inhibited by functional blocking antibodies against α_v, β_1, $\alpha_v\beta_1$, or free cRGD peptides by 30 to 60% (Fig. 1C). This inhibitory effect was not significant for C6-PLs or response to the addition of other functional blocking antibodies such as $\alpha_L\beta_2$, $\alpha_M\beta_2$, and $\alpha_4\beta_1$. This result demonstrates that both α_v and β_1 were essential subunits for the uptake of cRGDLs and that the free cRGD peptide competed with cRGDLs for the same sites on M/Ns. β_2-Integrins ($\alpha_L\beta_2$ and $\alpha_M\beta_2$) and $\alpha_4\beta_1$ are necessary for leukocyte (M/N) migration across the brain endothelium during an inflammatory response (*25*). Blocking antibodies against these integrins did not affect the cellular uptake efficiency of cRGDLs, which suggests that these integrins were not used during uptake. Therefore, cRGDL internalization was mainly mediated by the $\alpha_v\beta_1$ receptor and was not affected by the integrins related to inflammatory recruitment (*26*–*28*).

Comigration of cRGDLs with M/Ns across the BBB in vitro

To verify that the uptake of liposomes did not alter the chemotactic properties of M/Ns in response to inflammatory stimulation, a human brain microvessel endothelial cell (HBMEC) monolayer—a cell model of the BBB—was established on the upper chamber of a Transwell insert. A standard chemotactic factor [10^{-7} M *N*-formyl-methionyl-leucyl-phenylalanine (fMLP)] was added to the lower chamber under the HBMEC monolayers (*29*, *30*). The migrated cRGDLs in the lower chamber were significantly higher than migrated PLs in both neutrophils and monocytes (Fig. 1D). M/Ns efficiently carried cRGDLs through the simulated BBB, which resulted in up to an 18.6-fold increase in migrated C6-cRGDLs (with M/Ns) compared with that of C6-cRGDLs alone (without M/Ns). The ability of a few cRGDLs and PLs particles to cross the membrane alone indicated that the migration of liposomes was M/N dependent. Furthermore, the liposomes did not affect the degree of migration for M/Ns (fig. S5A), thereby confirming that the chemotaxis of M/Ns was not affected by the integrin $\alpha_v\beta_1$–mediated loading of liposomes. Furthermore, blocking intercellular adhesion molecule–1 (ICAM-1) or vascular cell adhesion molecule–1 (VCAM-1) (*26*–*28*) on the HBMEC substantially decreased the migration capacity of M/Ns (fig. S5B) and reduced the quantity of migrated liposomes carried by the cells (Fig. 1E).

Internalization of cRGDLs by M/Ns in vivo

To elucidate the in vivo fate of the liposomes, cRGDLs or PLs were labeled with hydrophilic Cy5 in the internal phase for tracking. Cy5-cRGDLs and Cy5-PLs were intravenously administered to rats that had suffered ischemia/reperfusion (I/R) injury—a well-established CI disease model—3 hours after reperfusion. Blood was sampled at prespecified time points, 1, 3, 5, 6, 8, and 12 hours after administration to assay the percentage of Cy5-positive neutrophils and monocytes present (Cy5-positive monocytes/total monocytes or Cy5-positive neutrophils/total neutrophils; Fig. 2A). The percentage of Cy5-positive monocytes in the cRGDL group was much higher than that of the PL group, regardless of the sampling time [i.e., initial (34.5%), valley time of 6 hours (23.5%), and 12 hours (average of 28.9%)], which resulted from the stronger and more rapid affinity of cRGDLs for monocytes than the other formulation. Although the affinity of PLs was also high initially, it continued to quickly decline after 1 hour. cRGDLs also exhibited higher affinity for neutrophils than PLs did, although there was initially no significant difference. Furthermore, cRGDLs exhibited much higher affinity for monocytes than it did for neutrophils, which was consistent with the results shown in Fig. 1B. Note that, monocytes were long lived, leading to the sustained targeted delivery of cRGDLs to the sites of inflammation in the brain. Although the uptake of PLs by monocytes was higher and lasted longer than that of the uptake by neutrophils, both neutrophils and monocytes are believed to be critical to delivery of liposomes to the brain because neutrophils compose a much higher percentage of white blood cells than monocytes (neutrophils: approximately 40 to 60% and monocytes: 2 to 9%).

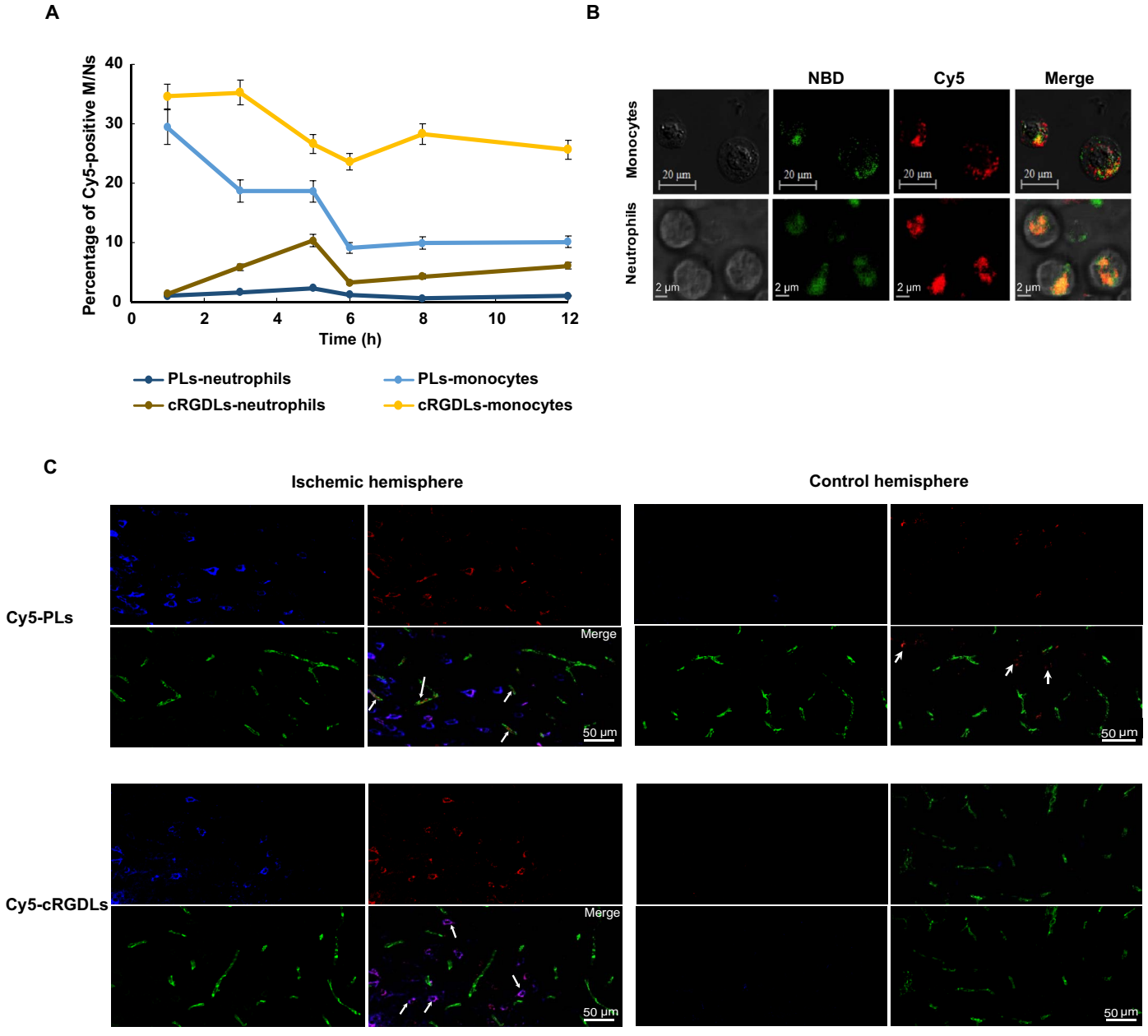

Fig. 2. The uptake of cRGDLs by M/Ns in vivo of I/R rats. (**A**) The percent of M/Ns loading with Cy5-cRGDLs in blood circulation of I/R rats assayed by flow cytometer (n = 3). (**B**) Confocal microscope images of cellular location of Cy5-NBD-cRGDLs in isolated M/Ns from I/R rats. Red: Cy5, hydrophilic core marker and green: NBD-PE, lipid membrane marker. (**C**) Confocal microscope images of comigration of Cy5-PLs/Cy5-cRGDLs with M/Ns across cerebral vessels in the ischemic hemisphere 12 hours after reperfusion. Blue: M/Ns stained with cell tracer CFSE; red: Cy5-PLs or Cy5-cRGDLs; and green: cerebral vessels labeled with vWF rabbit anti-rat antibody and secondary antibody of Alexa Fluor 594 goat anti-rabbit.

In addition, to visualize the localization of liposomes in M/Ns, cRGDLs or PLs were labeled with NBD-PE on the bilayer membrane of liposomes and loaded with hydrophilic Cy5 in the internal phase of liposomes. Isolated M/Ns from whole blood were visualized using CSLM (Fig. 2B). The colocalization of both markers (Cy5 and NBD-cRGDLs) was observed in M/Ns, where 80% of the Cy5 signal was overlaid with NBD signals according to analyses via ImageJ. The dual-labeling analysis of cellular levels confirmed that most of the cRGDLs were taken up and retained as intact nanocarriers by M/Ns, which is a critical step for successful brain-targeted delivery.

Comigration of liposomes with cell carriers across the BBB in vivo

To further confirm the comigration of liposomes with M/Ns in vivo, carboxyfluorescein diacetate succinimidyl ester (CFSE)–stained M/Ns and Cy5-cRGDLs or Cy5-PLs were consecutively administrated intravenously to I/R rats 12 hours after reperfusion. Brain tissue sections were stained with a von Willebrand factor (vWF) antibody to label the entirety of the vascular tree. In the ischemic hemisphere (Fig. 2C), Cy5-cRGDLs were mainly observed outside the vessels and colocalized with M/Ns. In contrast, less Cy5-PLs were observed in M/Ns because

the internalization into M/Ns was lower. Some Cy5-PLs were observed in the microvessels of the brain, indicating that more PLs were still in circulation. Few M/Ns were found in the nonischemic hemisphere, and much more PLs were observed there than cRGDLs. To further investigate the fate of liposomes, dual-label cRGDLs or PLs (Cy5-NBD-cRGDLs or Cy5-NBD-PLs) were administered to I/R rats 12 hours after reperfusion. The colocalization of Cy5 and NBD-PE in the ischemic hemisphere was consistently observed outside cerebral vessels for cRGDLs, whereas PLs were mainly confined in the vessels (fig. S6).

It has been reported that ischemic insults could induce the timely disruption of the BBB in both ischemic and nonischemic areas (*8*, *9*), which permitted the inflow of hematogenous fluid, possibly leading to the transport of noninternalized liposomes via blood flow. We subsequently carried out another experiment to examine the brain tissue sections 24 hours after reperfusion following the administration of CFSE-labeled M/Ns and Cy5-labeled liposomes. As a result, more Cy5-PLs were found inside and outside the vessels than cRGDLs in the nonischemic hemisphere (fig. S7). In the ischemic hemisphere, most of the Cy5-cRGDLs were concentrated on the M/Ns. On the contrary, very few PLs were trapped in the M/Ns, and many were scattered outside the M/Ns. Together, these results confirmed the hypothesis that most of the cRGDLs were internalized by M/Ns in the blood, carried across the BBB, and delivered to the ischemic area owing to the chemotactic nature of M/Ns. For PLs, a much lower internalization by immune cells resulted in a lower degree of accumulation in the ischemic area. Most of the PLs would remain in the blood in the early stage of reperfusion and then enter the brain with no selectivity when the permeability of BBB increased at a later stage of reperfusion.

Targeted delivery of cRGDLs by M/Ns to the ischemic brain and target cells

To investigate the temporal component of targeted delivery and the window of time for delivery—which depends on the secondary inflammatory signal after the onset of ischemia—we conducted a series of imaging studies using near-infrared fluorescent dye–labeled liposomes. The 1,1′-dioctadecyl-3,3,3′,3′-tetramethyl indotricarbocyanine iodide (DiR)–labeled cRGDLs (DiR-cRGDLs) or PLs (DiR-PLs) were administrated to a CI mouse model 0, 3, 6, 12, and 24 hours after reperfusion (Fig. 3A). Real-time fluorescence imaging acquired 1 hour after the administration of near-infrared fluorescent dye–labeled liposomes showed significant accumulation of DiR-cRGDLs as early as 3 hours after ischemic insult. The peak value was observed 24 hours after reperfusion, in agreement with a previous report that intraparenchymal granulocytes were numerous at 24 hours (*12*–*15*).

Consistent with the results of the microscopic imaging performed in the present study, (Fig. 2C and fig. S7), the accumulation of DiR-PLs in the ischemic region was extremely low owing to the low uptake efficiency of the M/Ns. However, the DiR fluorescence of PLs in the brain increased obviously after 24 hours of reperfusion, which might have been caused by BBB breakdown. It is consistent with the previous results of fig. S7. Sham nude mice and healthy mice exhibited few signals in the brain regardless of the type of liposome delivered, which confirmed that the inflammatory stimulation was the major driving force for targeted delivery. The few signals observed in the DiR control group also confirmed that the fluorescent signal was effectively tracking liposomes, not DiR itself. These results are in agreement with clinical observations that the secondary inflammation initiated at the early stage of CI onset, and the accumulation of blood-derived leukocytes in the ischemic region, lasts for more than 24 hours (*12*–*15*).

The mice treated 24 hours after reperfusion were euthanized 6 hours after the administration of liposomes. Brain tissues were imaged for fluorescent signals and then stained with 2,3,5-triphenyl tetrazolium chloride (TTC) after coronal brain sectioning to identify the ischemic region (identified by the presence of a white stain). The fluorescent signal area in rats that received DiR-cRGDLs overlapped with the white ischemic region to a great extent (Fig. 3B), indicating the selective and preferential accumulation of cRGDLs in the ischemic region. The fluorescent signal was much lower in DiR-PL–treated mice, as was the degree of overlap between the fluorescent signal and the white ischemic region. These results confirmed the capacity of immune cells to target specific tissues and also illustrated the intrinsic mechanism of action, which proved to be more effective than traditional nanoparticles for targeted drug delivery.

The dual-targeting effect on the ischemic region was further studied quantitatively using a radioactive tracer. I^{125}-labeled propyl gallate (I^{125}-PG) was loaded into PLs (I^{125}-PG-PLs) or cRGDLs (I^{125}-PG-cRGDLs) and then administered to I/R rats (equivalent to 55 μCi per rat) 1 hour after reperfusion (Fig. 3C). The ratio of reactivity between the ischemic and nonischemic hemispheres was calculated to indicate the selectivity of liposome distribution in the brain. As expected, the ratios of the sham-operated control and I^{125}-PG solution control were approximately 1 in all cases. In the I^{125}-PG-cRGDL group, the ratio ranged from 2.73 to 4.02 within 15 hours, demonstrating markedly improved accumulation in the ischemic brains. The highest ratio was observed 15 hours after the administration of I^{125}-PG-cRGDLs. In contrast, the ratio ranged only from 1.43 to 1.95 in I^{125}-PG-PL–treated rats within the first 3 hours and decreased to 1 in the next 12 hours, thereby implying the lack of selectivity of PLs at the later stage of ischemia. These results are consistent with the results we obtained from imaging (Fig. 3A and fig. S7).

Pharmacokinetics and biodistribution assay of PLs/cRGDLs in vivo

I^{125}-PG, I^{125}-PG-PLs, and I^{125}-PG-cRGDLs (equivalent to 55 μCi per rat) were administered to I/R rats 1 hour after reperfusion to investigate the pharmacokinetic and biodistribution of liposomes. Whole blood (0.5 ml) was drawn at 0.083, 0.5, 1, 3, 6, 12, and 24 hours after administration to determine radioactivity to elucidate pharmacokinetics. The high binding efficiency of cRGDLs with M/N led to an enhanced area under the curve (AUC), extended half time, and reduced clearance, in comparison to that observed with PLs and the PG group (Fig. 3D and table S2).

The heart, liver, spleen, lung, kidney, and brain were collected at 1, 6, 12, and 24 hours after administration to determine the radioactivity for biodistribution. The brain was divided into the left brain (ischemic hemisphere) and right brain (control hemisphere) for quantitative analyses on multitargeting effects (Fig. 3, E to H). Both PLs and cRGDLs exerted a profound influence on the biodistribution of PG. The increased accumulation of I^{125}-PG-cRGDLs was observed in the ischemic hemisphere during 24 hours, indicating an excellent multibrain targeting effect, which is consistent with our aforementioned results. I^{125}-PG-PLs that accumulated in the liver and the spleen were rapidly eliminated after 6 hours. A significant decrease in the accumulation of I^{125}-PG-cRGDLs in liver and the spleen in comparison to that of I^{125}-PG-PLs was observed 1 hour after administration, likely resulting from more binding with M/Ns in circulation. Most notably, the accumulation of I^{125}-PG-cRGDLs in the liver and the spleen was maintained at a very high level and was even much higher than that of I^{125}-PG-PLs

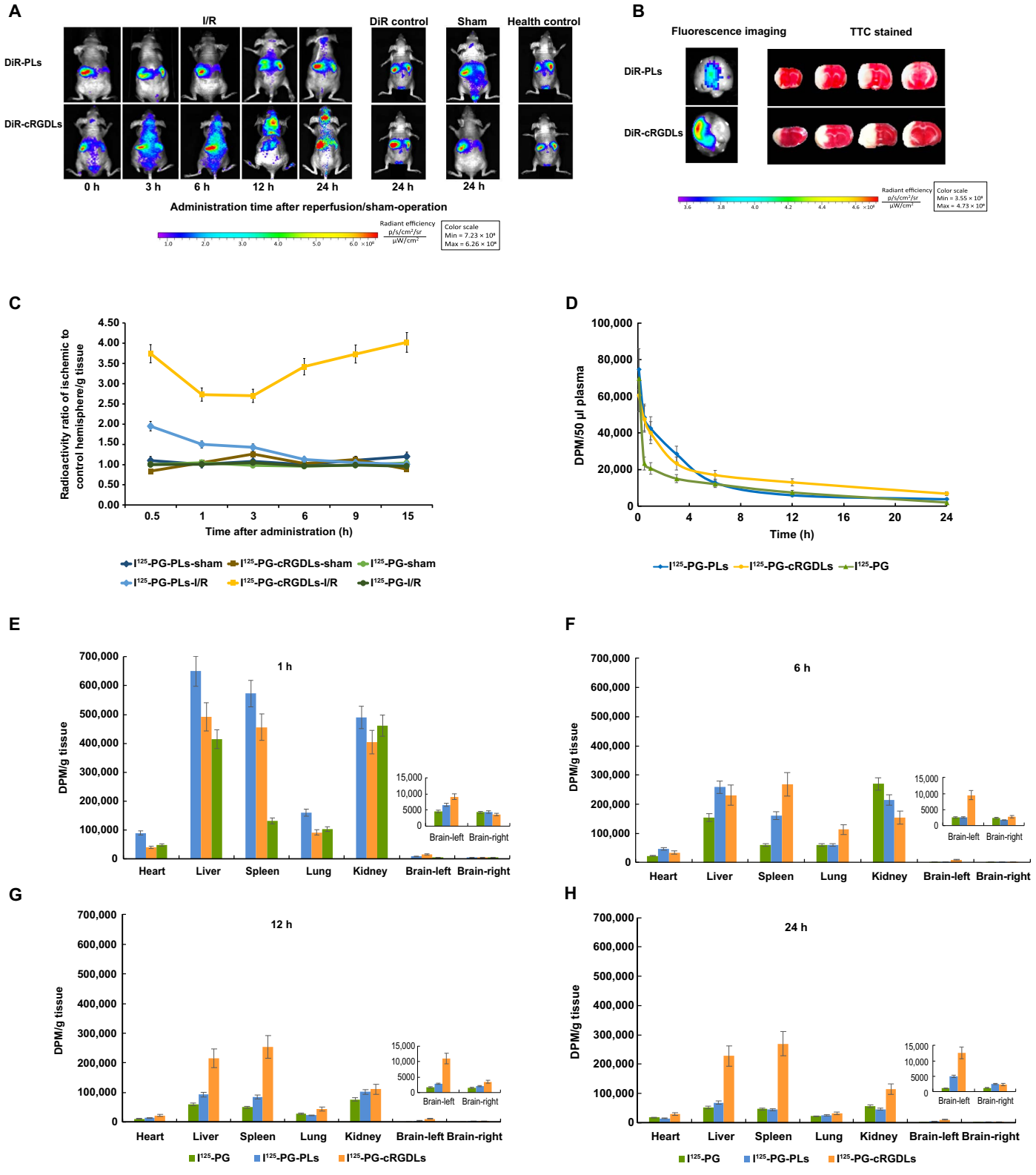

Fig. 3. Multitargeting delivery effect in vivo. (**A**) Fluorescence imaging of I/R nude mice after administration of DiR-cRGDLs/DiR-PLs at different times after reperfusion in I/R rat. (**B**) Coronal sections of TTC stain (white means ischemic area) or fluorescence imaging of I/R nude mice administrated with DiR-cRGDLs or DiR-PLs. (**C**) Radioactivity ratio of ischemic hemisphere to control hemisphere at different times after administration in I/R rats (n = 5). The bar represents 50 μm. (**D**) The plasma concentration-time curve and biodistribution (E) to (H) of I^{125}-labeled PLs, cRGDLs, and PG.

from 12 to 24 hours. It indicates that the elimination of cRGDLs in the liver and the spleen was slower than that of PLs. As the largest natural reservoir of immune cells, the spleen establishes critical connections with the ischemic brain during the progression of a stroke and mobilizes its cells to the site of injury in the ischemic brain, including neutrophils and monocytes/macrophages (*31*). Hence, we believe that some of the cRGDLs accumulated in the spleen bound with M/Ns via receptor-ligand interaction. Thus, lower spleen concentration of cRGDLs compared with PLs at the early stage resulted from binding with M/Ns in circulation; higher spleen concentration after 6 hours was due to binding with M/Ns in spleen. Together, those cRGDLs were continuously delivered to circulation and the ischemic brain by M/Ns released from the spleen, leading to enhanced AUC, extended half time, and continuous brain-targeted effects.

Note that slow clearance from the liver was observed in the I^{125}-PG-cRGDL group from 12 to 24 hours. Considering that αvβ1 integrins are expressed on hepatic stellate cells (*32*), this accumulation of cRGDLs is believed to be a result of preferred binding with stellate cells instead of Kupffer cells. Hence, cRGDLs are slowly eliminated by the liver.

Transport of liposomes from immune cell to target cell

To investigate the subsequent transport of liposomes from immune cells to target cells in the brain, dual-labeled cRGDLs or PLs (Cy5-NBD-cRGDLs or Cy5-NBD-PLs) were administered to I/R rats 12 hours

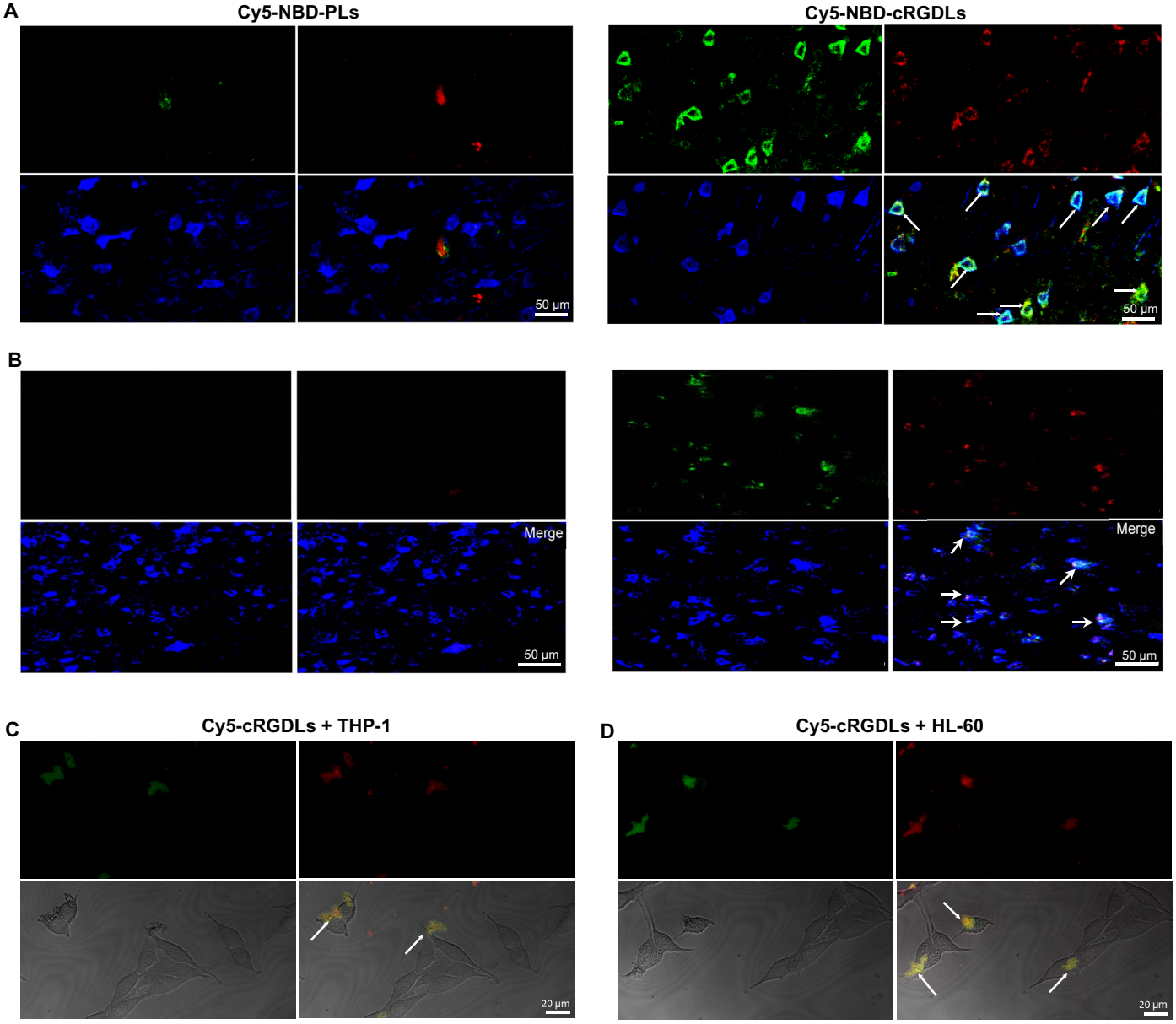

Fig. 4. The liposome transport from M/Ns to neuron in vitro and in vivo. (**A**) Confocal microscope images of colocation of Cy5-NBD-PLs/Cy5-NBD-cRGDLs with neurons or microglia (**B**) in brains of I/R rats 12 hours after reperfusion. Green: NBD-PE marker; red: Cy5 marker; blue: neurons stained with Rabbit anti-rat MAP2 or mouse anti-rat Iba-1 antibody and secondary antibody of Alexa Fluor 405 goat anti-rabbit. (**C**) Confocal microscope images of the transfer of Cy5-cRGDLs from THP-1 or (**D**) HL-60 to PC12. Green: THP-1 or HL-60 stained with Dil; red: Cy5-cRGDLs; PC12 was not stained.

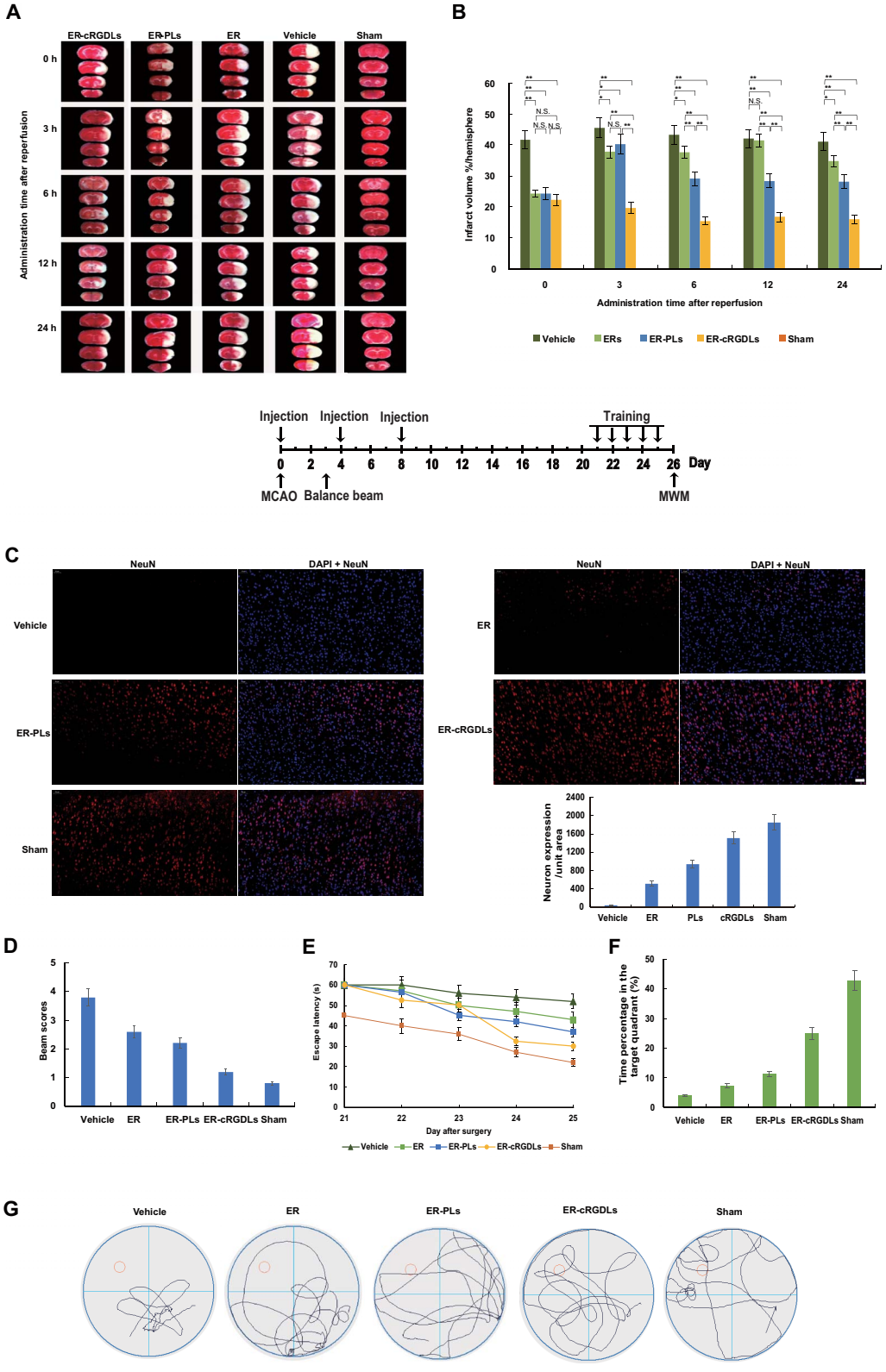

Fig. 5. Pharmacodynamic evaluation on liposome loading with ER in vivo. (**A**) Coronal sections stained with TTC of ischemic rats treated with liposomal ER 0, 3, 6, 12, and 24 hours after reperfusion. (**B**) Quantitative results of infarct volume of various formulations and control group. $^{**}P < 0.01$ and $^{*}P < 0.05$; N.S. means no significant difference. (**C**) Immunofluorescent labeling for NeuN in the cerebral cortex. The bar represents 50 μm. (**D**) Balance beam score of I/R rats treated with different formulations at 3 hours after reperfusion. (**E**) Latencies to find the hidden platform in the water maze during five consecutive training days. $n = 5$. (**F**) The percentage of time spent in the target quadrant within 60 s in the MWM test. $n = 5$. (**G**) Typical traces from a water maze experiment recorder. $n = 5$.

after reperfusion. Immunofluorescence of microtubule-associated protein 2 (MAP2 and ionized calcium binding adaptor molecule–1 (Iba-1) was used to identify neurons and activated microglia (*33*), respectively. Cy5-NBD-cRGDLs were observed in neurons (Fig. 4A) and activated microglia (Fig. 4B), indicating that the transfer of liposomes from leukocytes to target cells occurred. Endocytosis-independent mechanisms have been reported to likely be the main reason for the transport of liposomes between cells, involving the fusion of cellular membranes, exosomes, and macrophage bridging (*34*, *35*). To illustrate this mechanism, Cy5-cRGDLs were first loaded into DiI-labeled THP-1 cells (monocyte cell line) or HL-60 cells (neutrophil cell line). Subsequently, liposome-loaded immune cells were incubated with PC12 (neuronal cell line). The occurrence of both Cy5 and DiI signals in PC12 indicated the transfer of liposomes with immune cell membranes to neuronal cells (Fig. 4, C and D). Furthermore, bridges, membrane transfer, the deformation of immune cells, and the secretion of exosomes were also found in THP-1 or HL-60 (fig. S8). Although more studies are needed to elucidate the transport mechanism, the contact-directed transfer seemed to be an intrinsic behavior between immune cells and neuronal cells for material exchange, which was harnessed by cRGDLs for cell-targeted drug delivery.

Evaluation of neuroprotection by cRGDLs

We have proven that cRGDLs use immune cells as a vehicle to access ischemic regions of the brain, and thus, we have evaluated the therapeutic efficacy of cRGDLs encapsulating neuroprotective reagents in the treatment of CI. ER—a potent scavenger of hydroxyl radicals—was loaded into cRGDLs (ER-cRGDLs) or PLs (ER-PLs) with a 75% entrapment efficiency. The animals were administered intravenous injections of ER-cRGDLs, ER-PLs, and ER (all equivalent to 2 mg/kg ER) or saline solution (vehicle group) after 0, 3, 6, 12, and 24 hours of reperfusion. The infarction area (TTC stain) was visualized 48 hours after reperfusion and analyzed by ImageJ software (Fig. 5A). All the formations showed excellent protective effects when administrated immediately after reperfusion, and no significant differences were observed between the treatments, where the infarct volumes ranged from 53 to 58% of the control. This indicates that ER is a potent neuroprotective agent and that liposomal ER did not exhibit any advantage in comparison to ER at the early stages, as substantial neuroinflammation did not occur at 0 hours after reperfusion.

After 3 hours, ER did not exhibit substantial protective effects at any time in comparison to PLs and cRGDLs because of the difficulty of ER in reaching the lesion and damage tissues. PLs did not show significant differences in protective effects with ER at 3 hours after reperfusion and exhibited a stronger effect than ER after 6 hours. This was possibly due to the weak binding ability of PLs with neutrophils at 3 hours (Fig. 2A), as neutrophils are the main contributor at the early stages. After 6 hours, PLs exhibited a much stronger effect than did ER, owing to the increase in PLs to bind with monocytes, which was enhanced at later stages. The infarct volume of the ER-cRGDL–treated group after 3 hours was the lowest of all the groups at any time point, measuring 36 to 53, 49 to 59, and 40 to 52% of the control, ER-PLs, and ER groups, respectively (Fig. 5B). The therapeutic effect of ER-cRGDLs remained remarkable, although the mice were treated 24 hours after reperfusion. This result was quite consistent with that shown in Fig. 3A, where the CI-targeted delivery was triggered by inflammatory factors and displayed a wide therapeutic time window. This could potentially benefit patients with CI, who missed thrombolytic therapy as a result of the narrow therapeutic window.

For the treatment plan of administration 3 hours after reperfusion, immunofluorescent staining on neural nuclei (NeuN), a specific marker of mature neurons, in the cerebral cortex of the ischemic hemisphere was performed 24 hours after middle cerebral artery occlusion (MCAO) with one administration. Motor and cognitive performance was assayed by balance beam test (*36*) and Morris water maze (MWM) (*37*) on the 3rd or the 21st day after MCAO with three administrations. The great decrease in NeuN expression was observed in the vehicle group in comparison to the sham group. Increased expression of NeuN in ER and ER-PL groups was obtained compared with the vehicle group, indicating that both ER and ER-PLs had a neuron protection effect. The NeuN expression of ER-cRGDLs were much higher than that of ER and ER-PL groups, which indicated that better protection effect on neurons was expected for ER-cRGDLs (Fig. 5C).

To evaluate improvement in function outcomes, the balance beam test was performed 3 days after surgery. I/R injury robustly increased balance beam scores in the vehicle group. The PLs and ER groups significantly decreased the scores compared with the vehicle. The ER-cRGDL treatment exhibited the lowest score compared with PLs and ER, which indicates that the most improvement in balance function was obtained for the cRGDL group (Fig. 5D). For MWM test, rats were trained on the MWM task before the test. During the training trial, escape latencies gradually decreased in all groups. ER-cRGDLs showed lower escape latency compared with ER-PLs and ER during all the training trials and exhibited a sharp decrease in escape latency in the last 2 days (Fig. 5E). On the MWM test, the percentage of swimming time in the target quadrant was calculated for different formulations. The percentage of the ER-cRGDL group was higher than that of ER-PLs and ER, while ER-PLs also exhibited a better effect than ER (Fig. 5F). For the cRGDL group, we found more path in the target quadrant (Fig. 5G), which was consistent with time percentage results of Fig. 5F. Together, it indicates that a better memory was exhibited in the ER-cRGDL group. Hence, ER-cRGDLs greatly reduced spatial learning-memory impairment and balance function deficits.

Neuroinflammation, characterized by the recruitment of leukocytes, occurs in many neurological diseases, including ischemic stroke, Alzheimer's disease, glioma, and acquired immunodeficiency syndrome–related dementia (*38*, *39*). Here, a promising and broadly applicable strategy was elegantly designed and validated for the delivery drugs to brain lesions based on the high affinity of cRGD for neutrophils and monocytes. Our results show that the endogenous cell-mediated carrier system delivered cRGD-modified liposomes to lesions in an effective and sustainable manner and has the potential to greatly improve therapeutic outcomes. The transport mechanism of the system is distinct from current approaches to brain targeting, which are generally associated with sophisticated engineering and low targeting efficiencies (*40*). The elegant design, simple preparation process, and encouraging results of the delivery system presented in the present study provide an effective brain-targeting system that has potential, broad, and clinical applications for the treatment of various diseases related to inflammation.

MATERIALS AND METHODS

Reagents

SPC and DSPG were purchased from Lipoid Co. Ltd. DSPE-PEG (PEG-3400) was provided by AVT Pharmaceutical Co. Ltd. NBD-PE was purchased from Avanti Polar Lipid Inc. The cRGD was from GL

Biochem Ltd. ER (purity >98.5, production number MB1441) was purchased from Dalian Meilun Biotechnology Co. Ltd. Rabbit anti-rat vWF, rabbit anti-rat MAP2, mouse anti-rat Iba-1, ICAM-1, and VCAM-1 were from Abcam. Alexa Fluor 594 goat anti-rabbit, Alexa Fluor 405 donkey anti-mouse secondary antibody, and Alexa Fluor 405 goat anti-rabbit were used for fluorescence imaging. Antibodies for α_v, β_1, $\alpha_v\beta_1$, $\alpha_L\beta_2$, $\alpha_M\beta_2$, and $\alpha_4\beta_1$ were provided by Shanghai Perfect Biotech Co. Ltd. Fluorescence markers were provided by Fanbo Biochemicals Inc. Histopaque density gradient reagents and fMLP were from Sigma-Aldrich Co.

Cells and animals

The THP-1 (human acute monocytic leukemia cell line), PC12 cell line (a neuron-like rat pheochromocytoma cell line), HL-60 cell line (human promyelocytic leukemia cell line), and HBMEC were from American Type Culture Collection. Adult male Sprague-Dawley rats (250 to 300 g, 7 to 8 weeks) and male BALB/c nude mice (25 to 30 g, 7 to 8 weeks) were from Sino-British SIPPR/BK Lab Animal Co. Ltd. The animal experiment protocol was approved by the Animal Experimentation Ethics Committee of Fudan University.

Binding affinity assay with SPR

SPR was used to assay the binding affinity of cRGD peptide/cRGD-PEG-DSPE with αvβ1 protein by BIACORE T200. The experiment was performed on the research-grade CM5 sensor chip (carboxylated dextran surface) with the running buffer including HBS-EP [10 mM M Hepes (pH 7.4), 150 mM NaCl, 3 mM EDTA, and 0.005% polyoxyethylenesorbitan surfactant]. The αvβ1 protein was immobilized on the chip surface via amide linkages at pH 4.0. The analyte cRGD was diluted in HBS-EP buffer to a serial of concentrations from 0.039 to 20 μM and flowed over the αvβ1-immobilized CM5 chip to record resonance changes to assess binding affinity (Fig. 1A).

Uptake of liposomes by M/Ns

M/Ns were isolated from anticoagulant-treated rat peripheral blood within 2 hours of collection using the density gradient centrifugation method. C6-PLs or C6-cRGDLs (equivalent to 1 μM SPC) were incubated with monocytes or neutrophils (1×10^5 cells) for 30 min at 37°C. The C6 fluorescence intensity of M/Ns was determined by a flow cytometer with a sample voltage of 410 V. Blank M/Ns (not treated with liposomes) were used as a blank control (Fig. 1B).

For inhibition experiments, M/Ns (1×10^5 cells) were incubated at 37°C with free cRGD peptides (400 μg/ml) or antibodies for blocking individual functions (mouse anti-human α_v, β_1, $\alpha_v\beta_1$, $\alpha_L\beta_2$, $\alpha_M\beta_2$, and $\alpha_4\beta_1$) at 20 μg/ml for 30 min before the addition of C6-cRGDLs or C6-PLs. After 30 min of incubation, free liposomes and antibodies were removed, and the intensity of C6 fluorescence of the stained M/Ns was assayed by the flow cytometer with a sample voltage of 412 V. M/Ns untreated with antibodies were used as controls. Blank M/Ns, not treated with liposomes, were used as blank controls for flow cytometry (Fig. 1C).

For confocal images of PLs and cRGDLs internalized by M/Ns, cRGDLs or PLs were labeled with NBD-PE on the liposome bilayer membrane and loaded with hydrophilic Cy5 in the core for tracking purpose. After 30 min of incubation with Cy5-NBD-cRGDLs or Cy5-NBD-PLs, M/Ns were visualized using CSLM (fig. S10).

For uptake efficiency assay of the two liposomes in vitro, the M/Ns and Cy5-PLs/Cy5-cRGDLs (equivalently 1 μM SPC) were incubated for 30 min first. Then, free liposomes were removed by PBS wash and centrifugation. The original Cy5-PLs/Cy5-cRGDLs and stained M/Ns were subjected to an ultrasonic and Triton X-100 treatment for Cy5 fluorescence assay by microplate reader to determine the uptake efficiency in vitro according to Eq. 1

$$\text{Uptake efficiency} = \text{fluorescence intensity}_{M/N} / \text{fluorescence intensity}_{\text{liposomes}} \quad (1)$$

Comigration of liposomes with M/Ns in vitro

HBMEC, a cell model for BBB, was established on the upper chamber of a Transwell insert. C6-PLs or C6-cRGDLs (equivalent to 1 μM SPC) with M/Ns (1×10^5 cells) or without M/Ns were added onto the HBMEC monolayer, which had been pretreated with 10^{-7} M fMLP in the lower chamber. After 1 hour of incubation, the suspension in the lower chamber was collected and subjected to an ultrasonic treatment for C6 fluorescence assay using the microplate reader. Blank M/Ns (not treated with liposomes) were used as blank controls for cells, and non–fluorescence-labeled liposomes (PLs and cRGDLs) were used as a blank control for liposomes (Fig. 1D). The TEER (trans epithellal electric resistance) of the in vitro barrier model was monitored using a resistance instrument during the experiment (data are shown in fig. S9A).

Inhibition effect of liposomes on HBMEC

Functional blocking antibodies for mouse anti-human ICAM or VCAM at 20 μg/ml were preincubated with HBMEC (pretreated with 10^{-7} M fMLP in the lower chamber) for 30 min. Monocytes, neutrophils (1×10^5 cells), and C6-cRGDLs/C6-PLs (equivalent to 1 μM SPC) were added to the Transwells established for HBMEC. After 30 min of incubation, the lower chamber was subjected to ultrasonication and Triton X-100 treatment to assess C6 fluorescence assay by microplate reader. Blank M/Ns, untreated with liposomes, were used as a blank control for the microplate reader (Fig. 1E). The TEER of the in vitro barrier model was monitored using a resistance instrument during the experiments (data are shown in fig. S9B).

M/Ns (1×10^5 cells) were stained with CFSE and added onto the HBMEC (pretreated with 10^{-7} M fMLP in the lower chamber) with or without liposomes for 30 min of incubation. The migrated cells were collected and subjected to ultrasonication and Triton X-100 (2 mg/ml). Samples were taken at 10, 20, and 30 min for CFSE fluorescence assay by microplate reader to study any possible inhibitory effects of liposomes on cell migration. Blank M/Ns (not stained with CFSE) were used as blank controls for the microplate reader (fig. S5A). The TEER of the in vitro barrier model was monitored using a resistance instrument during the experiments (data are shown in fig. S9C).

In addition, CFSE-stained M/Ns were simultaneously added to the HBMEC with or without pretreatment with function-blocking antibodies for mouse anti-human ICAM or VCAM (20 μg/ml in the lower chamber). The fluorescence of migrated cells was also determined as previously mentioned. Blank M/Ns (not stained with CFSE) were used as blank controls for the microplate reader (fig. S5B). The TEER of the in vitro barrier model was monitored using a resistance instrument during the experiments (data are shown in fig. S9D).

In vivo uptake of liposomes with M/Ns

Cy5-NBD-PE-cRGDLs or Cy5-NBD-PE-PLs (equivalent to 26.5 mg SPC/kg) were administrated to I/R rats induced by the reperfusion of the MCAO. Blood of 200 μl was collected at the desired time points after

reperfusion, treated with 2 ml of red cell lysates for 5 min of incubation, and subsequently centrifuge at 3300 rpm. The supernatant was discarded, and the precipitate was resuspended for the collection of leukocytes. The percentage of dual-positive (Cy5 and NBD-PE) M/Ns in leukocytes were assayed by flow cytometer (Fig. 2A). Blood (1 ml) was collected at the end of the experiment for the isolation of neutrophils/monocytes using the density gradient centrifugation method and visualized by CSLM (Fig. 2B).

Transfer of liposomes from THP-1/HL-60 to PC12

THP-1 was stimulated every other day for 12 days with human interleukin-2 (100 U/ml). The HL-60 cell line was treated with 1.3% dimethyl sulfoxide for 96 hours, as previously reported to differentiate into polymorphonuclear-like cells. DiI was used to stain THP-1 or HL-60 as a membrane marker for 30 min, followed by DiI quenching before the experiment. Cy5-cRGDLs were incubated with THP-1 or HL-60 for 1 hour, and then the cRGDLs that were not taken up by the cells were completely removed. THP-1-cRGDLs or HL-6-cRGDLs (1×10^4 cell/cm^2) were added into the PC12 cells (1×10^4 cell/cm^2). After 1 hour of incubation, the interactions between cells were observed by CSLM.

Balance beam test

The beam balance test was carried out to investigate the motor coordination and balance of the rats. The rats took the test 3 days after MCAO. The performance was assessed using a five-point rating method (Fig. 5D).

MWM test

The spatial learning and memory abilities of the mice were examined by the MWM test. Rats were treated with different formulations on the fourth and eight day after the surgery. The training began on the 21st day after the surgery and consisted of four trials each afternoon for five consecutive days. The MWM test was performed on the 26th day (Fig. 5, E to G).

Statistical analysis

The data were expressed as means ± SD. The data were statistically analyzed using one-way or two-way analysis of variance (ANOVA) followed by Tukey's post hoc test. Values of $P < 0.05$ were considered statistically significant.

SUPPLEMENTARY MATERIALS

Supplementary material for this article is available at http://advances.sciencemag.org/cgi/content/full/5/7/eaau8301/DC1

Supplementary Materials and Methods

Fig. S1. The synthesis of cRGD peptide with PEG-DSPE assayed by MALDI-TOF.

Fig. S2. TEM photos and size distribution of various liposomes.

Fig. S3. Particle size of PLs/cRGDLs in different positon of the suspension or different medium by dynamic light scattering at different time.

Fig. S4. Derived count rate of PLs/cRGDLs in different positon of the suspension or different medium by dynamic light scattering at different time.

Fig. S5. The influence of liposomes and antibodies on the migration of M/Ns.

Fig. S6. Location of liposomes in ischemic brains of I/R rats 12 hours after reperfusion.

Fig. S7. Confocal microscope images of comigration of Cy5-PLs/Cy5-cRGDLs with M/Ns across cerebral vessels in the nonischemic hemisphere 24 hours after reperfusion.

Fig. S8. Transfer mechanisms of the liposomes from immune cells to neuron cells.

Fig. S9. TEERs of HBMEC in comigration and inhibition assay.

Fig. S10. Confocal microscope images of cellular location of Cy5-NBD-cRGDLs in M/Ns.

Table S1. Characterization of all liposomes used in the study.

Table S2. The pharmacokinetics parameters of I^{125}-labeled PG.

Reference (*41*)

REFERENCES AND NOTES

1. A. Denes, P. Thornton, N. J. Rothwell, S. M. Allan, Inflammation and brain injury: Acute cerebral ischaemia, peripheral and central inflammation. *Brain Behav. Immun.* **24**, 708–723 (2010).
2. A. Tuttolomondo, R. Di Sciacca, D. Di Raimondo, V. Arnao, C. Renda, A. Pinto, G. Licata, Neuron protection as a therapeutic target in acute ischemic stroke. *Curr. Top. Med. Chem.* **9**, 1317–1334 (2009).
3. M. Mokin, K. V. Snyder, A. H. Siddiqui, E. I. Levy, L. N. Hopkins, Recent endovascular stroke trials and their impact on stroke systems of care. *J. Am. Coll. Cardiol.* **67**, 2645–2655 (2016).
4. P. Khandelwal, D. R. Yavagal, R. L. Sacco, Acute ischemic stroke intervention. *J. Am. Coll. Cardiol.* **67**, 2631–2644 (2016).
5. A. D. Korczyn, M. Brainin, A. Guekht, Neuroprotection in ischemic stroke: What does the future hold? *Expert Rev. Neurother.* **15**, 227–229 (2015).
6. P. A. Lapchak, A critical assessment of edaravone acute ischemic stroke efficacy trials: Is edaravone an effective neuroprotective therapy? *Expert Opin. Pharmacother.* **11**, 1753–1763 (2010).
7. M. D. Ginsberg, Current status of neuroprotection for cerebral ischemia: Synoptic overview. *Stroke* **40**, S111–S114 (2009).
8. W. Xiaona, L. Yushan, S. Yanyun, L. Wenlan, J. Xinchun, *J. Neurol. Sci.* **363**, 63–68 (2016).
9. X. Jiang, A. V. Andjelkovic, L. Zhu, T. Yang, M. V. L. Bennett, J. Chen, R. F. Keep, Y. Shi, Blood-brain barrier dysfunction and recovery after ischemic stroke. *Prog. Neurobiol.* **163–164**, 144–171 (2018).
10. T. Wada, H. Yasunaga, R. Inokuchi, H. Horiguchi, K. Fushimi, T. Matsubara, S. Nakajima, N. Yahagi, Effects of edaravone on early outcomes in acute ischemic stroke patients treated with recombinant tissue plasminogen activator. *J. Neurol. Sci.* **345**, 106–111 (2014).
11. Z. Liu, M. Chopp, Astrocytes, therapeutic targets for neuroprotection and neurorestoration in ischemic stroke. *Prog. Neurobiol.* **144**, 103–120 (2016).
12. O. Y. Bang, B. Ovbiagele, D. S. Liebeskind, L. Restrepo, S. R. Yoon, J. L. Saver, Clinical determinants of infarct pattern subtypes in large vessel atherosclerotic stroke. *J. Neurol.* **256**, 591–599 (2009).
13. J. H. Garcia, K. F. Liu, Y. Yoshida, J. Lian, S. Chen, Influx of leukocytes and platelets in an evolving brain infarct (Wistar rat). *Am. J. Pathol.* **144**, 188–199 (1994).
14. N. V. Grønberg, F. F. Johansen, U. Kristiansen, H. Hasseldam, Leukocyte infiltration in experimental stroke. *J. Neuroinflammation* **10**, 115–123 (2013).
15. Q. Wang, X. N. Tang, M. A. Yenari, The inflammatory response in stroke. *J. Neuroimmunol.* **184**, 53–68 (2007).
16. X. Dong, D. Chu, Z. Wang, Leukocyte-mediated delivery of nanotherapeutics in inflammatory and tumor sites. *Theranostics* **7**, 751–763 (2017).
17. R. H. Andres, R. C. hoi, A. V. Pendharkar, X. Gaeta, N. Wang, J. K. Nathan, J. Y. Chua, S. W. Lee, T. D. Palmer, G. K. Steinberg, R. Guzman, The CCR2/CCL2 interaction mediates the transendothelial recruitment of intravascularly delivered neural stem cells to the ischemic brain. *Stroke* **42**, 2923–2931 (2011).
18. E. V. Batrakova, H. E. Gendelman, A. V. Kabanov, Cell-mediated drug delivery. *Expert Opin. Drug Deliv.* **8**, 415–433 (2011).
19. A. M. Brynskikh, Y. Zhao, R. L. Mosley, S. Li, M. D. Boska, N. L. Klyachko, A. V. Kabanov, H. E. Gendelman, E. V. Batrakova, Macrophage delivery of therapeutic nanozymes in a murine model of Parkinson's disease. *Nanomedicine (Lond.)* **5**, 379–396 (2010).
20. M. Barczyk, S. Carracedo, D. Gullberg, Integrins. *Cell Tissue Res.* **339**, 269–280 (2010).
21. A. S. Chung, Q. Gao, W. J. Kao, Either integrin subunit β1 or β3 is involved in mediating monocyte adhesion, IL-1β protein and mRNA expression in response to surfaces functionalized with fibronectin-derived peptides. *J. Biomater. Sci. Polym. Ed.* **18**, 713–729 (2007).
22. S. Najmeh, J. Cools-Lartigue, R. F. Rayes, S. Gowing, P. Vourtzoumis, F. Bourdeau, B. Giannias, J. Berube, S. Rousseau, L. E. Ferri, J. D. Spicer, Neutrophil extracellular traps sequester circulating tumor cells via β1-integrin mediated interactions. *Int. J. Cancer* **140**, 2321–2330 (2017).
23. R. Singh, T. Hui, A. Matsui, Z. Allahem, C. D. Johnston, M. Ruiz-Torruella, S. R. Rittling, Modulation of infection-mediated migration of neutrophils and CXCR2 trafficking by osteopontin. *Immunology* **150**, 74–86 (2017).
24. K. Anhalt, S. Geissler, M. Harms, M. Weigandt, G. Fricker, Development of a new method to assess nanocrystal dissolution based on light scattering. *Pharm. Res.* **29**, 2887–2901 (2012).
25. B. Engelhardt, H. Wolburg, Mini-review: Transendothelial migration of leukocytes: Through the front door or around the side of the house? *Eur. J. Immunol.* **34**, 2955–2963 (2004).
26. C. Weber, T. A. Springer, Interaction of very late antigen-4 with VCAM-1 supports transendothelial chemotaxis of monocytes by facilitating lateral migration. *J. Immunol.* **161**, 6825–6834 (1998).
27. G. Stoll, S. Jander, M. Schroeter, Inflammation and glial responses in ischemic brain lesions. *Prog. Neurobiol.* **56**, 149–171 (1998).

28. C. J. M. Frijns, L. J. Kappelle, Inflammatory cell adhesion molecules in ischemic cerebrovascular disease. *Stroke* **33**, 2115–2122 (2002).
29. E. Haber, E. Afergan, H. Epstein, D. Gutman, N. Koroukhov, M. Ben-David, M. Schachter, G. Golomb, Route of administration-dependent anti-inflammatory effect of liposomal alendronate. *J. Control. Release* **148**, 226–233 (2010).
30. W. Donald, R. Prameya, K. Dorovini-Zis, Adhesion and migration of polymorphonuclear leukocytes across human brain microvessel endothelial cells are differentially regulated by endothelial cell adhesion molecules and modulate monolayer permeability. *J. Neuroimmunol.* **184**, 136–148 (2007).
31. Z.-J. Liu, C. Chen, F.-W. Li, J.-M. Shen, Y.-Y. Yang, R. K. Leak, X.-M. Ji, H.-S. Du, X.-M. Hu, Splenic responses in ischemic stroke: New insights into stroke pathology. *CNS Neurosci. Ther.* **21**, 320–326 (2015).
32. N. I. Reed, H. Jo, C. Chen, K. Tsujino, T. D. Arnold, W. F. DeGrado, D. Sheppard, The $\alpha_v\beta_1$ integrin plays a critical in vivo role in tissue fibrosis. *Sci. Transl. Med.* **20**, **7**, 288ra79 (2015).
33. N. Zhang, M. Komine-Kobayashi, R. Tanaka, M. Liu, Y. Mizuno, T. Urabe, Edaravone reduces early accumulation of oxidative products and sequential inflammatory responses after transient focal ischemia in mice brain. *Stroke* **36**, 2220–2225 (2005).
34. M. J. Haney, Y. Zhao, S. Li, S. M. Higginbotham, S. L. Booth, H.-Y. Han, J. A. Vetro, R. L. Mosley, A. V. Kabanov, H. E. Gendelman, E. V. Batrakova, Cell-mediated transfer of catalase nanoparticles from macrophages to brain endothelial, glial and neuronal cells. *Nanomedicine (Lond.)* **6**, 1215–1230 (2011).
35. C. Zhang, C.-l. Ling, L. Pang, Q. Wang, J.-x. Liu, B.-s. Wang, J.-m. Liang, Y.-z. Guo, J. Qin, J.-x. Wang, *Theranostics* **7**, 3260–3275 (2017).
36. D. Liang, X.-B. He, Z. Wang, C. Li, B.-Y. Gao, J.-F. Wu, Y.-L. Bai, Remote limb ischemic postconditioning promotes motor function recovery in a rat model of ischemic stroke via the up-regulation of endogenous tissue kallikrein. *CNS Neurosci. Ther.* **24**, 519–527 (2018).
37. C. V. Vorhees, M. T. Williams, Morris water maze: Procedures for assessing spatial and related forms of learning and memory. *Nat. Protoc.* **1**, 848–858 (2006).
38. J. A. Smith, A. Das, S. K. Ray, N. L. Banik, Role of pro-inflammatory cytokines released from microglia in neurodegenerative diseases. *Brain Res. Bull.* **87**, 10–20 (2012).
39. V. H. Perry, D. C. Anthony, S. J. Bolton, H. C. Brown, The blood-brain barrier and the inflammatory response. *Mol. Med. Today* **8**, 335–341 (1997).
40. R. Jin, G. Yang, G. Li, Inflammatory mechanisms in ischemic stroke: Role of inflammatory cells. *J. Leukoc. Biol.* **87**, 779–789 (2010).
41. G. Jonsdottir, I. E. Ingolfsdottir, F. R. Thormodsson, P. H. Petersen, Endogenous aggregates of amyloidogenic cystatin C variant are removed by THP-1 cells in vitro and induce differentiation and a proinflammatory response. *Neurobiol. Aging* **34**, 1389–1396 (2013).

Acknowledgments

Funding: This work was supported by the National Natural Science Foundation of China (no. 81673372, 81773911, and 81690263), Asia 3 Foresight Program (no. 81361140344), the Opening Project of Key Laboratory of Drug Targeting and Drug Delivery System, Ministry of Education (Sichuan University), and the Development Project of Shanghai Peak Disciplines-Integrative Medicine (no. 20180101). **Author contributions:** J.Q. and Jianxin Wang conceived and designed the experiments; J.Q., J.H., X.Y., S.L., Z.C., C.Z., M.L., H.R., J.L., and Jue Wang performed all the experiments; J.Q., Jianxin Wang, Y.W., and J.Z. wrote the manuscript; all authors analyzed and discussed the data. **Competing interests:** The authors declare that they have no competing interests. **Data and materials availability:** All data needed to evaluate the conclusions in the paper are present in the paper and/or the Supplementary Materials. Additional data related to this paper may be requested from the authors.

Submitted 20 July 2018
Accepted 3 June 2019
Published 10 July 2019
10.1126/sciadv.aau8301

Citation: J. Hou, X. Yang, S. Li, Z. Cheng, Y. Wang, J. Zhao, C. Zhang, Y. Li, M. Luo, H. Ren, J. Liang, J. Wang, J. Wang, J. Qin, Accessing neuroinflammation sites: Monocyte/neutrophil-mediated drug delivery for cerebral ischemia. *Sci. Adv.* **5**, eaau8301 (2019).